Diamond & Related Materials 76 (2017) 115–122

Contents lists available at ScienceDirect

Diamond & Related Materials

journal homepage: www.elsevier.com/locate/diamond

Investigations of the co-doping of boron and lithium into CVD diamond thin films

S.C. Halliwell[a,b], P.W. May[a,*], N.A. Fox[b], M.Z. Othman[a,c]

[a] School of Chemistry, University of Bristol, Bristol BS8 1TS, United Kingdom
[b] H.H. Wills Physics Laboratory, University of Bristol, Bristol BS8 1TL, United Kingdom
[c] Faculty of Science & Technology, Islamic Science University of Malaysia, Nilai, Malaysia

ABSTRACT

Lithium has been incorporated into heavily boron-doped single-crystal (SCD), microcrystalline (MCD) and nanocrystalline diamond (NCD) films at concentrations up to $\sim 2 \times 10^{20}\,cm^{-3}$ using Li_3N as a solid-state Li source for in-diffusion and diborane as the B source. The quality, morphology, electrical resistance and concentration of B and Li dopants present in a range of B + Li co-doped SCD, MCD and NCD films have been studied. Analysis of the SIMS depth profiles for Li enabled the diffusion constants, *D*, to be measured (in units of $cm^2\,s^{-1}$) as: 2.5×10^{-15}, 1.3×10^{-14} and 7.0×10^{-14} for SCD, MCD and NCD, respectively, at 1100 K. The value for *D* for SCD agrees closely with that in the literature, while the much larger values for the polycrystalline films provide direct evidence that Li can diffuse rapidly along or through diamond grain boundaries at elevated temperatures. If prolonged diffusion allows the Li to reach the Si substrate, the Si acts as a sink for Li absorbing large quantities and reducing its concentration in the diamond film.

1. Introduction

Diamond films grown by chemical vapour deposition (CVD) are finding an increasing number of applications due to the superlative properties of diamond coupled with their rising availability and affordability from a number of commercial suppliers [1]. Doping the diamond with boron allows p-type material to be deposited, with films ranging in conductivity from highly insulating to near metallic [2] or even superconducting [3], and this has enabled the fabrication of many simple p-type devices, such as sensors. In contrast, finding a dopant for diamond that imparts n-type semiconducting characteristics suitable for use in electronic devices has proven to be elusive [4]. Nitrogen is one possible dopant, and nitrogen-doped diamond has been successfully synthesised using hot-filament (HF) CVD and microwave plasma CVD (MWCVD) techniques [5,6]. However, the N donor level in diamond is too deep to be useful in electronic devices [7]. Alternatively, phosphorus has been used to successfully n-dope CVD diamond films [8], but the films are not sufficiently conducting for many device applications. Due to its low work-function [9], lithium has also been suggested as a possible shallow n-type dopant [10,11], although it is mobile in diamond above 400 °C so is prone to diffusion, and can form electrically inactive Li clusters. Because there are very few volatile organo-Li compounds, many of which are unstable on contact with air or water vapour, adding Li to the CVD gas mixture has proven difficult [12]. Solid-state diffusion using Li vapour or various lithium oxides into SCD has been reported with diffusion constants $\sim 10^{-15}$–$10^{-14}\,cm^2\,s^{-1}$ [13]. However, an earlier report [14] gave values for the diffusion constant that were nearly an order of magnitude smaller than these, as well as a smaller activation barrier for diffusion. It was suggested [13] that these earlier results may have been underestimated due to the presence of high Li concentrations found at the surface, possibly as a result of ineffective cleaning of the surface or clustering of Li near the surface. More recently, Othman et al. [15] reported that in-diffusing lithium into an already nitrogen-doped microcrystalline diamond (MCD) film enabled Li to be incorporated into the diamond at concentrations $\sim 5 \times 10^{19}\,cm^{-3}$. The N atoms were believed to immobilize the Li and prevent aggregation [16,17]. However, the high electrical resistance of the doped films, despite the high Li and N concentrations, suggested that most of the Li and N atoms were trapped as electrically inactive species. In related theoretical work [18], co-doping of diamond with both N and Li has been predicted to produce an n-type material for a Li:N ratio of 1:4, although achieving this experimentally has yet to be demonstrated.

Taken together, these findings suggest that co-doping with suitably chosen dopants might be a new and promising avenue of research for solving the n-doping problem. This report focuses on the preparation

* Corresponding author.
E-mail address: Paul.May@bristol.ac.uk (P.W. May).

http://dx.doi.org/10.1016/j.diamond.2017.05.001
Received 28 February 2017; Received in revised form 20 April 2017; Accepted 2 May 2017
Available online 03 May 2017

and characterization of B + Li co-doped diamond. The idea is that substitutional B atoms may immobilize one or more Li atoms in a similar manner to N. Although each B acceptor should electrically compensate for each Li donor, we now investigate whether the ratio of Li:B could be used to control the overall conductivity, with B-rich films being p-type and Li-rich films possibly being n-type.

1.1. Experimental

Two different substrate types were used, upon which a range of diamond samples were deposited. Polycrystalline diamond (PCD) films were deposited onto 1 cm^2 single-crystal boron-doped Si wafers (100), which had been manually abraded with 1–3 μm diamond particles prior to diamond growth. In contrast, single-crystal diamond (SCD) layers were grown on high-pressure high-temperature (HPHT) SCD (3 × 3 mm^2) type 1b (100) substrates (purchased from Element Six, Ltd.) which had been previously cleaned in a 50:50 mixture of concentrated nitric acid and sulfuric acid to remove any non-diamond material. No extra seeding or abrasion was necessary to initiate diamond nucleation on these SCD substrates.

Diamond was grown using a hot filament CVD system and standard diamond CVD conditions [1]. During growth, three tantalum filaments were positioned 3 mm from the substrate surface and were electrically heated to 2100–2200 K measured using a 2-colour optical pyrometer. The substrates were heated by proximity to the filaments as well as by an independent heater, and the deposition temperature was kept constant at ~1100 K. The process pressure was held constant at 20 Torr, while the input gas consisted of a mixture of methane, hydrogen and diborane (B_2H_6). A mixing ratio of 1%CH_4 in H_2 produced MCD films while 4%CH_4 in H_2 produced nanocrystalline diamond (NCD) films. The diborane flow determined the doping level of the film: 'lower B-doped diamond' was achieved for a mixing ratio of 20 ppm B_2H_6 in H_2 (i.e. a gas-phase B:C ratio of 0.4% for MCD and 0.1% for NCD) while 'higher B-doped diamond' was achieved for a mixing ratio of 120 ppm B_2H_6 in H_2 (i.e. a gas-phase B:C ratio of 2.4% for MCD and 0.6% for NCD). Note that both these doping levels can be considered ‘heavily’ doped as they result in B concentrations in the films (> 10^{20} cm^{-3}) which are above that needed for metallic conductivity.

These conditions deposited either MCD films with faceted crystallites ~1–5 μm in size, or NCD films with rounded, ‘cauliflower’ crystallites ~100 nm in size, depending upon the gas mixture used (see Table 1). Films were grown for 3 h making them ~1.75–2 μm thick. The same process conditions for MCD growth were also used to grow diamond on the SCD substrates. Because the growth conditions were not optimised to grow single-crystal diamond, some renucleation was inevitable, even on an SCD substrate. However, this unwanted effect was kept to a minimum by careful process control and by keeping the deposited layer < 1 μm in thickness. Nevertheless, the as-grown layers were not perfectly epitaxial, and had a small number of grain boundaries, albeit several orders of magnitude fewer than the PCD films. Nevertheless, we shall still refer to them as SCD layers, bearing in mind the above considerations.

Table 1
Details of 2-point resistance, *R*, for the lower (L) and higher (H) B-doped MCD & NCD films after different volumes of Li_3N were in-diffused. The MCD films were 1.75 μm thick while the NCD films were all 1.85 μm thick. The capping layers were 0.2–0.3 μm for all films.

Sample	Volume of Li_3N diffused/μl	Initial B-doping	Grain type	*R*/Ω
A	0	L	MCD	51.2
B	100	L	MCD	101.9
C	150	L	MCD	61.1
D	200	L	MCD	95.1
E	0	H	MCD	23.8
F	100	H	MCD	50.9
G	150	H	MCD	43.2
H	200	H	MCD	65
I	0	L	NCD	813.5
J	100	L	NCD	2942
K	150	L	NCD	3618
L	200	L	NCD	5075
M	0	H	NCD	83.8
N	100	H	NCD	211.2
O	150	H	NCD	276.9
P	200	H	NCD	295.5

To incorporate Li into the diamond films, commercially available lithium nitride (Li_3N) powder (CERAC, 99.5% purity, 250 μm particle size) was used as a source. The Li_3N was first prepared as a stable liquid suspension; 85 mg of Li_3N was dispersed in 5 ml of chloroform (chosen due to its polarity and non-oxidising properties), to which 5 mg of polyoxyethylene ether (POE) was added to increase the stability of the suspension. This mixture was then sonicated for 1 h to ensure a homogeneous suspension.

The prepared suspension of Li_3N was drop-cast onto the pre-grown B-doped diamond thin films. For the larger area PCD films on Si, either 100, 150 or 200 μl of suspension was drop-cast depending on the Li doping level required. Because the SCD substrates had only 7% of the area of the PCD films, proportionately less Li_3N suspension was required. It was calculated that diffusing ~7 μl of Li_3N solution into these smaller SCD samples gave an estimated surface density for Li_3N of 1.9 mg cm^{-2}, which was comparable to 1.7 mg cm^{-2} when diffusing 100 μl into the larger samples. Once the liquid had dried, the sample was then placed in the HFCVD reactor and heated to a substrate temperature of approximately 1100 K in an H_2 atmosphere for 1 h. This melted the Li_3N powder, allowing the Li to diffuse from the surface into the diamond to depths that could be estimated from secondary ion mass spectrometry (SIMS) measurements. It was assumed that because the signal from N was below the SIMS detection limit, either the N present in the Li_3N evaporated as N_2 during the process or it was incorporated at a negligible level. After diffusion, either an undoped diamond or B-doped diamond capping layer typically 0.2 μm thick was grown on top of the sample, using the same conditions as before, in order to encapsulate the co-doped region and ensure subsequent SIMS measurements were as accurate as possible.

In later experiments, multiple layers of Li were diffused into B-doped diamond in a multi-step process. To deposit these, the processes of drop-casting the Li_3N solution, heating to diffuse the Li into the diamond, and then embedding the Li in a layer of diamond, were repeated sequentially as many times as required, with the final step being a diamond capping layer as before.

The film morphology, quality and dopant concentration were investigated using scanning electron microscopy (SEM), Raman spectroscopy and SIMS depth profiling, respectively. The SIMS system comprised a focused 25 keV gallium ion gun (FEI electronically variable aperture type operating with a beam current of 3 nA) fitted to a Vacuum Generators model 7035 double-focusing magnetic sector mass analyser with a channeltron ion detector [19]. This system detected lithium as Li^+ and boron as B^+. These ion intensities were monitored alongside C^+, which acted as a constant when calculating absolute concentrations of atoms using a SCD calibration sample that had previously been implanted with a known concentration of B and Li. The minimum detection limit of B in the system was 2.20 × 10^{18} cm^{-3} and for Li was 2.03 × 10^{17} cm^{-3}. Oxygen was monitored in these films as O^+ ions to ensure that counts of Li^+ were not mistakenly enhanced by the presence of oxygen [20,21,22]. It has previously been found that sample roughness does not affect how distinct the boundaries appear between layers present in the sample because this particular SIMS set-up planarises the initial surface morphology [15]. This is also why a capping layer helps during analysis, because the capping layer planarised first before reaching the co-doped area.

In the case of thermal diffusion from a constant source, the diffusion

coefficient, D, was determined by fitting the SIMS depth profile obtained by SIMS to Eq. (1) [13]:

$$N(x,t) = N_0\left(1 - \mathrm{erf}\frac{x}{2\sqrt{Dt}}\right) \quad (1)$$

where t was the total time for which the sample was heated (usually 1 h diffusion plus 15 mins for the deposition of the capping layer), N is the concentration of Li at a distance x, with N_0 being the maximum peak height which occurs at $x = 0$ where the original Li suspension was placed.

Resistance values of different films were also obtained using a combination of 2-point probe and van der Pauw measurements, depending on the substrate. For all MCD and NCD samples, electrical resistance measurements were obtained using a 2-point probe technique. First, two 1 mm × 1 mm silver contacts were deposited onto the film surface with a separation of 7 mm using physical vapour deposition (PVD). Then the exposed diamond surface was oxygen terminated using an ozone treatment lamp. This ensured that electrical measurements came from the diamond bulk and were not affected by surface conductivity arising from surface transfer doping [23]. However, the possibility still arises that some fraction of the conductivity measured in this manner results from conduction through the Si substrate rather than from the diamond layer. For 2-point measurements, substrate effects can never completely be eliminated, and so the *absolute* values for conductivity are unreliable. However, because the Si substrates were all cut from the same Si wafer, substrate conductivity effects should be identical for each sample, and so the *relative* conductivity values should give a reliable indicator of the differences in conductivity between samples. For the same reason, van der Pauw measurements were not performed on these samples due to the conductivity of the B-doped Si substrate confounding the measurements.

In contrast, SCD samples allowed both the 2-point probe and the 4-point probe van der Pauw resistance measurements to be taken because the insulating undoped SCD substrate ensured only the newly deposited co-doped diamond layer was measured. The four silver contacts (labelled 1–4 in a counter-clockwise direction) used here were 0.2 mm × 0.2 mm in size and separated by 0.5 mm at the four corners of the sample. The sheet resistance, R_S, of each sample was calculated by first finding R_A and R_B using Eqs. (2) and (3) [24,25].

$$R_A = (R_{21,34} + R_{12,43} + R_{43,12} + R_{34,21})/4 \quad (2)$$

$$R_B = (R_{32,41} + R_{23,14} + R_{14,23} + R_{41,32})/4 \quad (3)$$

where $R_{ab,cd}$ means that a positive direct current was injected into contact a and taken out from contact b, while the d.c. voltage was measured between contacts c and d. This was then used to calculate R_S using the van der Pauw Eq. (4).

$$\exp\left(-\pi R_A/R_S\right) + \exp\left(-\pi R_B/R_S\right) = 1 \quad (4)$$

2. Results and discussion

2.1. Film quality and morphology

Raman spectroscopy was performed using He–Cd 325 nm wavelength excitation, with a laser spot diameter and focusing depth resolution of ~1 μm. This means that the overall Raman spectra obtained from all the films (Fig.1) contain signal components from the capping layer plus the Li + B doped region, and possibly also from the bulk substrate. The spectra show the expected typical features [26] for SCD, MCD and NCD. The peak at 1332 cm^{-1} is due to the sp^3-hybridised C in diamond, while the broad peak around 1580 cm^{-1} (G-band) arises due to the graphitic, sp^2-hybridised C found within the grain boundaries of PCD. The intensity ratio of the diamond peak to that of the G-band provides an estimate of the quality of diamond thin film.

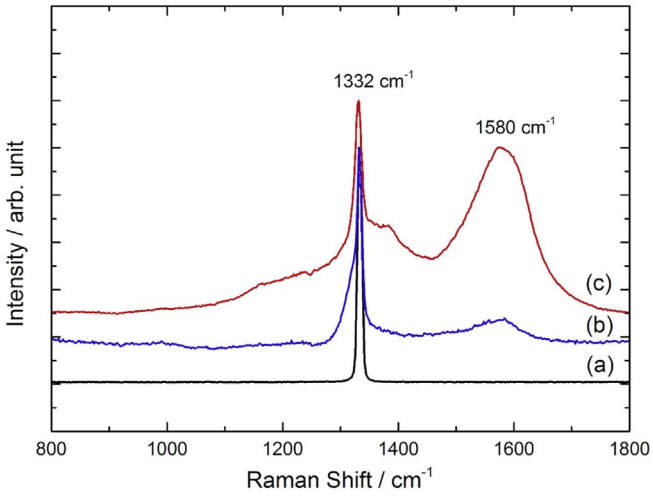

Fig. 1. Laser Raman spectra from lower B-doped (a) SCD, (b) MCD and (c) NCD films. Curves (b) and (c) have been offset vertically for clarity.

Figs.2(a) and (b) show Raman spectra for higher B-doped MCD and NCD, respectively, taken before, as well as after, Li_3N was diffused into the film. It appears that after Li was diffused there was a small improvement in the quality of these diamond samples, with the Raman spectra showing an increase in the diamond:G-band intensity ratio. As suggested previously [15], the diffusion of Li may preferentially etch the graphitic carbon at grain boundaries and, in this case, could also remove some of the inactive boron in the grain boundaries. The improvement in diamond quality is most evident in the Raman spectra of NCD films (Fig.2(b)), which shows a significant increase in diamond:G-band intensity ratio. This is consistent with NCD films having a greater proportion of grain boundaries.

The B-doped diamond films showed the characteristic spectra previously reported by others [27,28,29,30,31,32,33], whereby the first-order diamond phonon peak becomes asymmetric. This so-called Fano line shape is due to the diamond phonon undergoing a quantum mechanical interference with the continuum of electronic states induced by the presence of the dopant, in this case B [34,35,36]. The Raman spectra of higher B-doped films contain a broad peak at 1225 cm^{-1}; this can be attributed to the relaxation of selection rules allowing more diamond phonons to become Raman active [27,28,29,35]. Unfortunately, due to these distortions in the shape and width of the Raman features it was difficult to see if any new peaks corresponding to B or Li were present.

From previous studies [2] we know that the ratio of CH_4:H_2 is responsible for a change in crystallite size; the low flow rate of diborane used in this study has no affect upon grain size. SEM micrographs shown in Fig.3(a) confirm that the higher B-doped MCD sample is, indeed microcrystalline, with many twinned facetted crystallites - a feature which has been noted by other studies of similar films [37,38]. After Li in-diffusion (Fig.3(b)) the only change in diamond surface morphology is that there appears to be a slight smoothing along the facet edges and vertices. This was also observed by Othman et al. [15] who ascribed it to preferential etching of sp^2 carbon at grain boundaries and edges by Li. Similarly, Fig.3(c) shows the higher B-doped NCD film, with its typical cauliflower morphology [2]. Again, after Li in-diffusion (Fig.3(d)) there is a slight smoothing of the edges and vertices. With volumes of Li_3N suspension > 200 μl the etching became more significant leading to extensive damage to the film in the form of holes, pitting or corrosion. For this reason, Li_3N suspension volumes used for doping experiments never exceeded 200 μl.

Two-point probe measurements (Table 1) showed that film resistance was a function of many parameters. The first factor is the CH_4 flow rate used during growth as this changed the morphology of the

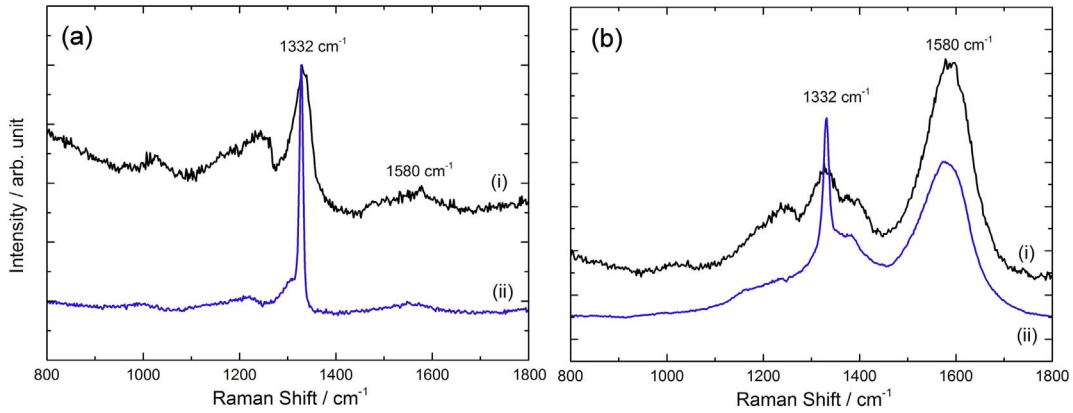

Fig. 2. Laser Raman spectra from (a) a higher B-doped MCD film (i) before and (ii) after 150 μl Li_3N had been in-diffused, and (b) a higher B-doped NCD film (i) before and (ii) after 200 μl Li_3N had been in-diffused.

resulting film from facetted MCD to cauliflower NCD. The MCD films generally had lower resistance than the NCD films, for the same B doping level. This is possibly due to the larger number of grain boundaries in NCD films, which cause scattering of electrons and may also provide sites where many of the B atoms can reside in electrically inactive sites, making the boron doping much less efficient [2].

For the same film type, as expected [19,32,39], the lower B-doped films had greater resistance than the higher B-doped films. When compared to B-doped diamond, the B + Li co-doped films had higher resistance. This was more noticeable in the NCD samples, where a consistent trend was observed whereby the film resistance increased with the volume of Li_3N in-diffused (see Table 1 samples J, K, L, N, O and P). One reason for this increase in resistance could be that the added Li was compensating for some of the B. Alternatively, it could be because the Li atoms are diffusing along the grain boundaries and etching them to some extent (as seen in the SEM images in Fig.3). It is known that the sp^2-hybridised C present in the grain boundaries improves electrical conduction within PCD via an electron hopping mechanism [2,40,41,42]. With some of the sp^2-hybridised C being etched, electrical conductivity would decrease. This is consistent with the NCD films, with their larger number of grain boundaries, showing a greater resistance increase after Li addition than the MCD films. This model also suggests that the Li within the grain boundaries is presumably electronically inactive, and not all Li that diffuses into the diamond lattice may occupy electronically active sites.

2.2. Changing dopant concentrations

SIMS depth profiling was used to measure the concentration of both B and Li within the diamond films as a function of depth below the surface. The film thicknesses were previously measured using cross-sectional SEM, and these values were used to calibrate the SIMS etch rate into an accurate depth measurement. The measured B concentration is directly linked to the flow rate of diborane used during growth. Samples grown with the higher flow rate of diborane have an average boron concentration of 2.9×10^{21} cm^{-3}, with all samples in the range of 1×10^{21} to 9×10^{21} cm^{-3}. Samples grown with the lower flow rate of diborane produce an average B concentration of 4.9×10^{20} cm^{-3} with all samples in the range of 2×10^{20} cm^{-3} to 9×10^{20} cm^{-3}. All films contain B concentrations well above the detection limit of the SIMS system (2.2×10^{18} cm^{-3}). The SIMS system detects secondary ions emitted from an area of approximately 30 μm × 30 μm, such that

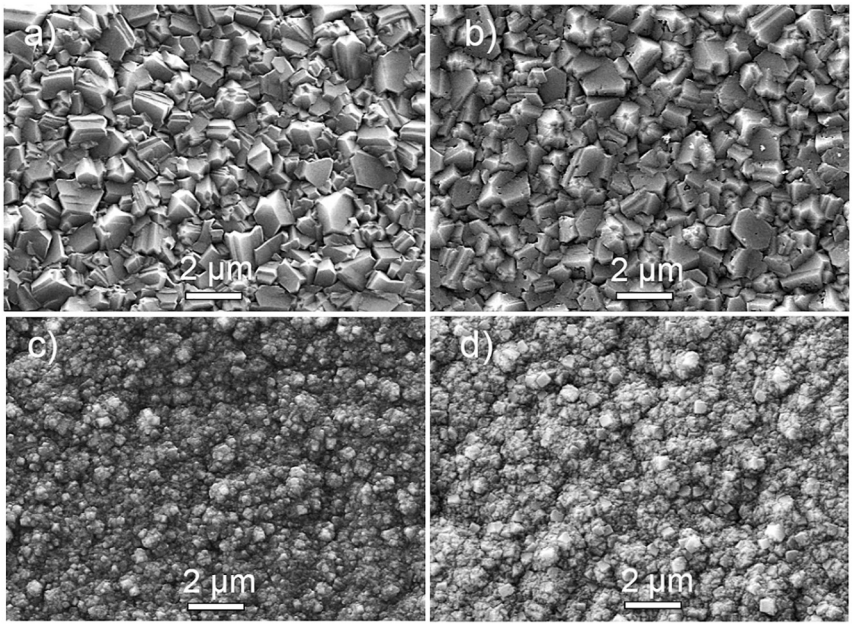

Fig. 3. SEM micrographs showing the typical facetted structure of B-doped MCD (a) before, and (b) after in-diffusion of 100 μl Li_3N, and the typical cauliflower morphology of B-doped NCD (c) before, and (d) after 100 μl Li_3N diffusion. In both film types there is very little noticeable change in overall morphology due to the in-diffusion process, except for some smoothing or rounding of the edges and vertices, possibly due to etching of the sp^2 carbon by Li [15].

any concentrations calculated using SIMS are an average over this area, incorporating a large number of diamond crystals and grain boundaries. This means that any differences in concentration in grain boundaries and within the diamond lattice will not be distinguished. In all films characterised with SIMS there is an overlap region where both B and Li can be found, so potentially a truly co-doped area exists in each film.

Determining the concentration of Li is more difficult because the diffusion process leads to a characteristic Gaussian depth profile in which there is a peak concentration of Li diffused over approximately the first ~600 nm of the original B-doped film and also into the undoped capping layer. Deeper than 600 nm the Li concentration becomes almost constant but remains above the detection limit for all MCD and NCD films, indicating the Li diffused through the entire film to the Si substrate in all PCD samples. To analyse the concentration profiles, two parameters have been defined (i) the maximum Li concentration, measured at the peak position of the respective concentration curve, and (ii) the average Li concentration for the bulk of the film, which is the concentration of Li averaged over all depths 600 nm and deeper.

Further investigation shows that the concentration of B present within the films does not appear to affect the Li concentrations detected. This can be seen in Figs.4(a) and (b), which show the SIMS depth profiles of NCD with higher (a) and lower (b) B doping, respectively. Both samples were diffused with 100 μl of Li_3N resulting in fairly similar maximum Li concentrations of 2.03×10^{19} cm^{-3} and 2.85×10^{19} cm^{-3}, respectively. The maximum Li concentrations is mainly affected by the volume of Li_3N diffused into the diamond film, and not the morphology of the diamond. This can be seen in Figs.4(c) and (d) where both films were lower B-doped MCD, but the sample in Fig.4(d), with a maximum Li concentration of 1.13×10^{20} cm^{-3}, had twice the volume of Li_3N in-diffused than that of Fig.4(c), with a maximum Li concentration of 4.23×10^{19} cm^{-3}. For both NCD and MCD films the average Li concentration detected at the maximum was ~3.4 times higher when the volume of Li_3N diffused was doubled from 100 μl to 200 μl (Table 2).

Table 2
Li concentrations at the peak maximum, and the average throughout the rest of the PCD films.

Grain type	Volume of Li_3N diffused/ μl	Maximum Li concentration detected/ (10^{19} cm^{-3})	Average Li concentration in bulk/ (10^{19} cm^{-3})
MCD	100	3.56	0.12
NCD	100	2.34	1.03
MCD	200	11.6	0.94
NCD	200	8.26	0.66

Table 3
Range of maximum Li concentrations and average Li concentration throughout the rest of the PCD film, for various B + Li co-doped diamond film samples.

Grain Type	Volume of Li_3N diffused/ μl	Range of maximum Li concentrations detected /(10^{19} cm^{-3})	Range of Li concentrations in the bulk /(10^{19} cm^{-3})
MCD	100	2.72–4.96	0.0789–0.169
NCD	100	1.39–3.03	0.570–1.83
MCD	200	1.71–25.3	0.290–1.52
NCD	200	3.00–17.5	4.87–8.92

Despite this apparent trend for both MCD and NCD samples, the same cannot be said for the Li concentrations deeper into the films. For MCD films, the average bulk Li concentration increases by an even greater amount when the Li_3N volume is doubled (~8.7×), yet in the NCD films the average Li bulk concentration decreased when the volume of Li_3N was increased from 100 μl to 200 μl. Because of this seemingly contradictory trend it is important to look at the range of Li concentrations detected in all films analysed using SIMS. Table 3 shows that there is a large range of maximum Li concentrations detected for each type of sample, with many of the ranges overlapping, regardless of the volume of Li_3N solution used, B concentration or morphology of the

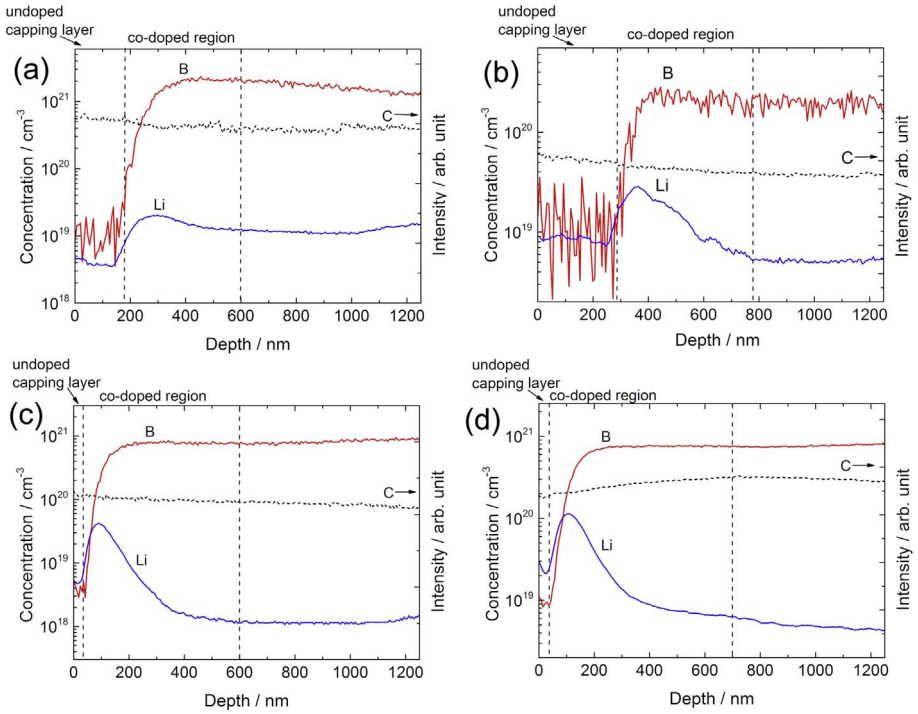

Fig. 4. SIMS depth profile of B + Li co-doped films with different morphologies grown on a Si substrate (top 1250 nm only) followed by an undoped diamond-capping layer. (a) 1.85-μm-thick higher B-doped NCD, 100 μl Li_3N, (b) 1.85-μm-thick higher B-doped NCD, 100 μl Li_3N, (c) 1.75-μm-thick lower B-doped MCD with 100 μl Li_3N diffused and (d) 1.75-μm-thick lower B-doped MCD with 200 μl of Li_3N diffused. Shown on the plot are the calibrated concentrations of Li and B (left-hand axis) and C intensity (right-hand axis), as a function of depth beneath the diamond surface.

sample.

We believe an explanation for why Li bulk concentration was not affected by the volume of Li_3N added in NCD, but was in MCD, could lie in the ability of the Si substrate to act as a sink for Li [43]. Being 0.5 mm thick, the Si substrate readily absorbs any Li that reaches it, and so the Li concentration profile of the diamond film depends upon how quickly the Li can diffuse through it to reach the Si substrate.

To quantify this further, the diffusion constants were calculated by fitting the SIMS depth profiles to Eq.(1), giving values of $1.3 \times 10^{-14}\,cm^2\,s^{-1}$ and $7 \times 10^{-14}\,cm^2\,s^{-1}$ for the MCD and NCD films, respectively. These values are significantly larger than the corresponding value for SCD, measured by ourselves (see later) and Uzan-Saguy et al. [13], of $2.5 \times 10^{-15}\,cm^2\,s^{-1}$. We can further assume that Li diffusion follows an Arrhenius-like dependence upon temperature [14]

$$D = D_0 \exp\left(\frac{-E}{k_B T}\right) \tag{5}$$

where E is the activation barrier for diffusion (in eV), k_B is the Boltzmann constant and T is the temperature (in our case 1100 K), and the pre-exponential factor D_0 is the 'ballistic' diffusion constant, i.e. the value when there is no activation barrier or impediment to diffusion. A similar approach was adopted by Uzan-Saguy et al. [13] to calculate values for the activation barrier as a function of temperature, with values around 0.26 eV being found for Li in SCD. Using the value of D for SCD, along with $E = 0.26$ eV and the deposition temperature of 1100 K, we obtain $D_0 = 3.9 \times 10^{-14}\,cm^2\,s^{-1}$. Comparing this to the values of D for MCD and NCD it is clear that the value of D for MCD is comparable in magnitude to D_0, whereas that for NCD far exceeds it. This is clear evidence that a different diffusion mechanism must operate in MCD and NCD compared to that in SCD - one which allows the Li atoms to diffuse ~5 or ~28 times faster, respectively, than in SCD.

These findings are all consistent with the idea that Li can diffuse more quickly through grain boundaries than in bulk diamond. Because NCD has a much greater proportion of grain boundaries than MCD, the Li can rapidly diffuse through the entire NCD film to be lost into the Si substrate. In contrast, in MCD the Li diffuses more slowly through the scarcer grain boundaries, so less is lost to the Si substrate. This may also give more of an opportunity for Li to diffuse into the diamond crystallites. The peak concentration of Li was not as affected by the diamond crystal size because it occurs at a depth corresponding to the original Li_3N drop-casting site. As there was excess Li present at that position, more than could diffuse through the diamond or grain boundaries within the diffusion time, increasing the volume of Li_3N drop-cast simply increased the concentration of Li detected there. The large range of this Li maximum concentration (Table 3) was mainly due to variations in the procedure used to drop-cast the Li_3N solution; as the chloroform evaporated the Li_3N powder in the solution tended to move and this led to a slightly non-uniform concentration of Li being deposited. So despite Table 2 showing that, on average, the larger the volume of Li_3N used the higher the concentration of Li detected at both the maximum and throughout the sample, this result must be treated with caution suggesting that a more uniform Li distribution method is required.

2.3. Single-crystal diamond samples

To further study the role of grain boundaries in Li diffusion, it was decided that B + Li co-doped SCD films would be deposited onto SCD substrates, meaning no (or negligible) grain boundaries were present either in the film or substrate. The use of a SCD substrate also eliminated the unwanted sink for Li diffusion observed when using the previous Si substrates. Three SCD samples were grown on SCD substrates, with sample R being lower B-doped and samples Q (a control sample) and S being higher B-doped, as before. Samples R and S then had 7 μl of Li_3N diffused into them, followed by a capping layer of undoped diamond, although this layer may become slightly doped during deposition by diffusion of Li and/or B from the layer below. The SIMS depth profiles for sample R presented in Fig.5 show that Li can still diffuse through the diamond lattice, even with no grain boundaries present to help the diffusion. However, the width of the Li peak was much sharper and slightly narrower for SCD, and the Li diffused over only ~350 nm, compared to the peak covering ~500 nm in the PCD films (see Fig.4). Moreover, for the PCD samples the Li level remained above the detection limit once it levelled out after the peak, but in the SCD samples the Li concentration drops below the detection limit. Fitting the Li depth profile in Fig.5 to Eq. (1) gave a value for the SCD diffusion constant of $2.5 \times 10^{-15}\,cm^2\,s^{-1}$ at 1100 K, which agrees with that of ref. [13].

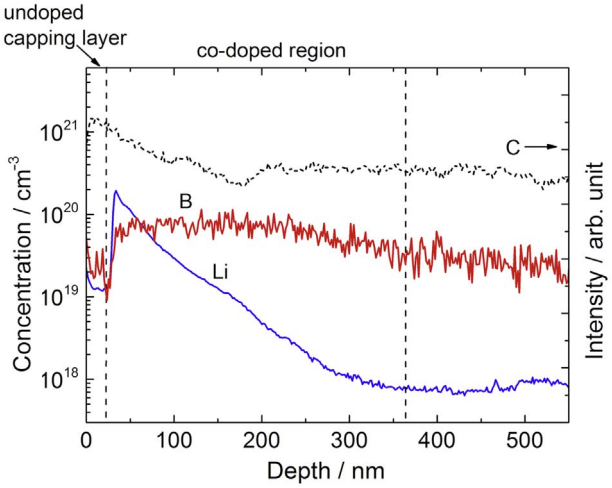

Fig. 5. SIMS depth profile of a B + Li co-doped SCD film (sample R) grown on an undoped SCD substrate (top 700 nm shown). Shown on the plot are the calibrated concentrations of Li and B (left-hand axis) and C intensity (right-hand axis), as a function of depth beneath the diamond surface.

The two-point probe method and the van der Pauw method were used to calculate the resistance and the sheet resistance, R_S, respectively, of SCD samples Q, R and S, and are given in Table 4. The highly B-doped control with no Li (sample Q), had a very low resistance value, which, as expected, was somewhat lower than the values measured for the equivalent PCD control samples E and M given in Table 1. After Li doping (sample S), the film resistance had increased by 50–80%. Although no lightly B-doped SCD control sample was measured, from previous results it is reasonable to assume that such a film would have a resistance similar to, or probably lower than, that of the equivalent MCD control (sample A in Table 1) of ~50 Ω. After Li doping (sample R), however, the resistance was ~4 kΩ. For both lightly and heavily B-doped films, therefore, the process of Li addition increases the film resistance.

Table 4 also shows that the values for R_A and R_B are almost identical for sample Q, but vary by ~20% for samples R and S. This indicates that the Li co-doped films were quite inhomogeneous, most likely due to the uneven distribution, and consequently, diffusion, of Li_3N.

Table 4
Calculated values for the 2-point resistance, R, and van der Pauw values for R_A, R_B and R_S for SCD samples Q, R and S. In all samples the film thickness was 0.8 μm epitaxially grown onto a SCD substrate, with an undoped capping layer 25–30 nm thick.

Sample	Initial B doping	R/Ω	R_A/Ω	R_B/Ω	R_S/(Ω □$^{-1}$)
Q	H	–	6.8	6.9	3.1
R	L	3440	4088	3453	17050
S	H	68	83	68	340

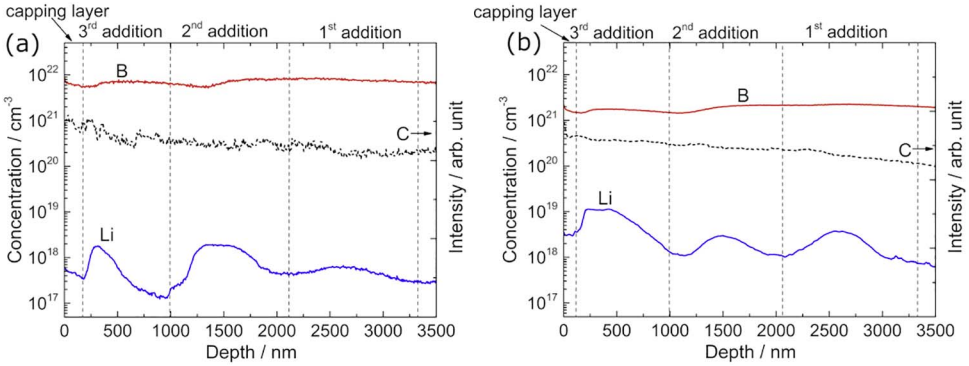

Fig. 6. SIMS depth profile of 3-layered B + Li co-doped MCD film grown on a Si substrate (top 3500 nm only). The resulting film was ~3.6 μm thick. Shown on the plot are the calibrated concentrations of Li and B (left-hand axis) and C intensity (right-hand axis), as a function of depth beneath the diamond surface. (a) Sample T with 100 μl of Li_3N diffused each time, (b) Sample U with 200 μl of Li_3N diffused each time.

Because of this difference in values, the van der Pauw Eq. (3) for R_S was solved iteratively rather than using an approximation, giving sheet resistance values of 17 kΩ $\square^{-1}$ for sample R and 340 Ω $\square^{-1}$ for sample S. This is consistent with the SIMS analysis which found that sample R had an average B concentration of 5.83×10^{19} cm^{-3} while sample S had an average of 1.77×10^{20} cm^{-3}.

2.4. Multiple layers

The samples analysed using SIMS in Fig.6 had three sequential Li_3N-diffusion + diamond-growth steps, with 1 μm of B-doped diamond grown at each stage and a final 150 nm B-doped diamond capping layer. As expected, the SIMS depth profiles show 3 distinct Li layers present in the films, with the breadth of the peaks providing an indication of the amount of Li diffusion that has occurred. The deepest Li layer had the longest time to diffuse, as during each subsequent diffusion and growth process, the Li diffused both downwards towards the Si substrate and upwards into the newly grown diamond layer. As a result, the SIMS feature associated with this deep layer is rather broad (~1200 nm). The SIMS peak from second-deepest Li layer is sharper (~1000 nm), while that from the topmost Li layer is quite sharp and distinct (~900 nm). This clearly shows that the longer the diffusion period, the broader the diffusion width. It is unknown whether the B and Li move into more stable clusters within the diamond lattice, or the Li continues to diffuse throughout the diamond and grain boundaries. Some of the Li may also be diffusing out of the diamond and into the Si substrate sink.

Two such multilayered films were constructed on a heavy B-doped MCD-on-Si substrate using different volumes of Li_3N in each diffusion process. Fig.6(a) shows SIMS analysis from a sample with 100 μl of Li_3N added each time (sample T) while Fig.6(b) is from one with 200 μl of Li_3N added at each diffusion (sample U). The maximum Li concentrations measured by SIMS in sample T were: 1st addition (which is deepest in the film, closest to the substrate) ~6.60×10^{17} cm^{-3}, 2nd addition ~1.91×10^{18} cm^{-3} and 3rd addition ~1.79×10^{18} cm^{-3}. When double the volume of Li_3N was diffused (sample U) the maximum Li concentrations detected were: 1st addition ~3.76×10^{18} cm^{-3}, 2nd addition ~2.98×10^{18} cm^{-3} and 3rd addition ~1.14×10^{19} cm^{-3}. This shows the longer the diffusion time, usually the smaller the maximum Li concentration detected, indicated by the SIMS depth-profile peak becoming wider but shorter.

3. Conclusions and future work

Lithium and boron have both been incorporated into NCD, MCD and SCD films without causing significant changes to the observed diamond morphology using Li_3N as a solid source of Li for in-diffusion and B_2H_6 as a gaseous source of B. SIMS analysis has shown that B and Li are incorporated into diamond with both elements being present at high concentrations within the same region. No nitrogen was detected in the films above the SIMS detection limit, indicating that the N from the Li_3N had not been incorporated in the film but had been pumped away, probably as gaseous N_2. However, electrical resistance measurements show that conductivity in all of the co-doped film remains dominated by the B acceptors, although the process of addition of Li to the films does increase the resistance significantly. This could be a result of the added Li donors compensating for some of the B acceptors. However, a more likely explanation is that introduction of a large number of Li atoms at a specific location results in the localised disruption of the diamond lattice. At high temperatures, the Li diffuses downwards into the film below and upwards into the growing capping layer, and so the distortion to the diamond lattice may be partially mitigated. Nevertheless, the diamond film as a whole is less perfect than it was before the Li addition, and this decreases the conductivity.

It remains unclear whether the Li occupies substitutional, interstitial, or grain boundary sites, or a mixture of all three. Measurements of the diffusion constant for Li in SCD at 1100 K agree with those reported previously, while those for MCD and NCD are respectively 5 and 27 times larger. This provides clear evidence that a different migration mechanism operates for Li in polycrystalline diamond films to that in SCD, with grain boundary transport being the likely route. The rapid transport of Li through grain boundaries is a particular problem for PCD films grown on Si substrates - the likely substrate of choice for any semiconductor devices applications - because the Si acts as a sink for the Li, absorbing it from the diamond, and thus decreasing the Li concentration within the film. The implications are that that the Si substrate could effectively absorb *all* the Li given a chance; if the film is maintained at 1100 K for long enough, eventually *all* the Li would diffuse out of the diamond and into the Si. In contrast, for freestanding PCD films, maintaining the films at 1100 K for long periods of time would instead result in a homogeneous distribution of Li throughout the film. This would also be true of freestanding SCD samples, although due to the much slower diffusion rate this equilibration would require a much longer time period. It also brings into question the longevity of Li-doped diamond, especially PCD, devices at elevated temperatures. It would be useful to repeat these diffusion measurements at a range of different temperatures, allowing the activation barriers for the various diffusion processes in SCD and PCD to be determined.

The fact that the values measured for the diffusion constant in our boron-doped diamond are consistent with those measured by others in undoped diamond suggests that *in situ* B does not inhibit Li diffusion, and so does not significantly pin down Li atoms preventing them from clustering, as originally hoped. However, we are unable to determine from these data whether the migrating Li atoms remain isolated or cluster together. This question may be answered by detailed modelling of Li defects in diamond using solid-state computer codes such as

CASTEP and CRYSTAL. Nevertheless, these findings together suggest that it is increasingly unlikely that Li, either alone or as part of a co-doping scheme, will make an effective n-dopant for diamond. The quest for an n-dopant for diamond may require the use of more unusual dopant/co-dopant schemes, including various combination of N, Ca, Al, Mg and other potential donor atoms, which we suggest as a direction for future research in this area.

Acknowledgements

With thanks to James Smith, Liam Payne and Peter Heard for their invaluable help and advice, the facilities at the Interface Analysis Centre at the University of Bristol and EPSRC DTA award EP/K502996/1 for funding this project. We also thank Xian Zhang for the resistance data for sample Q. Supplementary material and raw data for this report can be found in the University of Bristol data repository: DOI: http://dx.doi.org/10.5523/bris.20y9s3hoxu2h25v7h3ru38i15.

References

[1] P.W. May, Diamond thin films: a 21st century material, Phil. Trans. R. Soc. Lond. A 358 (2000) 473–495.
[2] P.W. May, W.J. Ludlow, M. Hannaway, P.J. Heard, J.A. Smith, K.N. Rosser, Raman and conductivity studies of boron-doped microcrystalline diamond, facetted nanocrystalline diamond and cauliflower diamond films, Diam. Relat. Mater. 17 (2008) 105–117.
[3] Y. Takano, M. Nagao, I. Sakaguchi, M. Tachiki, T. Hatano, K. Kobayahi, H. Umezawa, H. Kawarada, Superconductivity in diamond thin films well above liquid helium temperature, Appl. Phys. Lett. 86 (2004) 2851–2853.
[4] R. Kalish, Doping of diamond, Carbon 37 (1999) 781–785.
[5] V. Baranauskas, B.B. Li, A. Peterlevitz, M.C. Tosin, S.F. Durrant, Nitrogen-doped diamond films, J. Appl. Phys. 85 (1999) 7455–7458.
[6] W. Muller-Sebert, E. Worner, F. Fuchs, C. Wild, P. Koidl, Nitrogen induced increase of growth rate in chemical vapor deposition of diamond, Appl. Phys. Lett. 68 (1996) 759–760.
[7] R. Kalish, C. Uzan-Saguy, B. Philosoph, V. Richter, J.P. Lagrange, E. Gheeraert, A. Deneuville, A.T. Collins, Nitrogen doping of diamond by ion implantation, Diam. Relat. Mater. 6 (1997) 516–520.
[8] A. Lazea, V. Mortet, J. D'Haen, P. Geithner, J. Ristein, M. D'Olieslaeger, K. Haenen, Growth of polycrystalline phosphorous-doped CVD diamond layers, Chem. Phys. Lett. 454 (2008) 310–313.
[9] P.A. Anderson, The work function of lithium, Phys. Rev. 75 (1949) 1205–1207.
[10] J.P. Goss, R.J. Eyre, P.R. Briddon, Theoretical models for doping diamond for semiconductor applications, Phys. Status Solidi B 245 (2008) 1679–1700.
[11] J.P. Goss, P.R. Briddon, Theoretical study of Li and Na as n-type dopants for diamond, Phys. Rev. B 75 (2007) 075202.
[12] K. Okumura, J. Mort, M. Machonkin, Lithium doping and photoemission of diamond thin films, Appl. Phys. Lett. 57 (1990) 1907–1909.
[13] C. Uzan-Saguy, C. Cytermann, B. Fizgeer, V. Richter, R. Brener, R. Kalish, Diffusion of lithium in diamond, Phys. Status Solidi 193 (2002) 508–516.
[14] J. te Nijenhuis, G.Z. Cao, P.C.H.J. Smits, W.J.P. van Enckevort, L.J. Giling, P.F.A. Alkemade, M. Nesládek, Z. Remeš, Incorporation of lithium in single crystal diamond: diffusion profiles and optical and electrical properties, Diam. Relat. Mater. 6 (1997) 1726–1732.
[15] M.Z. Othman, P.W. May, N.A. Fox, P.J. Heard, Incorporation of lithium and nitrogen into CVD diamond thin films, Diam. Relat. Mater. 44 (2014) 1–7.
[16] A. Namba, Y. Yamamoto, H. Sumiva, Y. Nishibayashi, T. Mai, Process for producing n-type semiconductor diamond, United States Pat, US 0177962 (A1) (2006).
[17] A. Namba, T. Imai, H. Takeuchi, Low resistivity n-type semiconductor diamond and method of its manufacture, United States Pat, US 7255744 (B2) (2007).
[18] M.Z. Othman, Studies of n-type doping and surface modification of CVD diamond for use in thermionic applications (PhD Thesis), University of Bristol, U.K., June 2014.
[19] P.J. Heard, K.A. Feeney, G.C. Allen, P.R. Shewry, Determination of the elemental composition of mature wheat grain using a modified secondary ion mass spectrometer (SIMS), Plant J. 30 (2001) 237–245.
[20] C.A. Anderson, Progress in analytic methods for the ion microprobe mass analyser, Int. J. Mass Spectrom. Ion Phys. 2 (1969) 61–74.
[21] G. Blaise, M. Bernheim, Adsorption of gases studied by secondary ion emission mass spectrometry, Surf. Sci. 47 (1975) 324–343.
[22] T. Sakamoto, B. Tomiyasu, M. Owari, Y. Nihei, Ambient oxygen effect in Ga + FIB-SIMS, Surf. Interface Anal. 22 (1994) 106–110.
[23] V. Baranauskas, B.B. Li, A. Peterlevitz, M.C. Tosin, S.F. Durrant, Nitrogen-doped diamond films, J. Appl. Phys. 85 (1999) 7455–7458.
[24] L.J. van der Pauw, A method of measuring specific resistivity and hall effect of discs of arbitrary shape, Phillips Res. Rep. 13 (1958) 1–9.
[25] L.J. van der Pauw, A method of measuring the resistivity and hall coefficient on lamellae of arbitrary shape, Phillips Tech. Rev. 20 (1958) 220–224.
[26] P.W. May, W.J. Ludlow, M. Hannaway, P.J. Heard, J.A. Smith, K.N. Rosser, Raman and conductivity studies of boron doped microcrystalline diamond, facetted nanocrystalline diamond and cauliflower diamond films, Chem. Phys. Lett. 446 (2007) 103–108.
[27] E. Gheeraert, P. Gonon, A. Deneuville, L. Abello, G. Lucazeau, Effect of boron incorporation on the “quality” of MPCVD diamond films, Diam. Relat. Mater. 2 (1993) 742–745.
[28] M. Bernard, C. Baron, A. Deneuville, About the origin of the low wave number structures of the Raman spectra of heavily boron doped diamond films, Diam. Relat. Mater. 13 (2004) 896–899.
[29] F. Pruvost, E. Bustarret, A. Debeuville, Characteristics of homoepitaxial heavily boron-doped diamond films from their Raman spectra, Diam. Relat. Mater. 9 (2000) 295–299.
[30] E. Bustarret, E. Gheeraert, K. Watanabe, Optical and electronic properties of heavily boron-doped homo-epitaxial diamond, Phys. Stat. Sol. (A) 199 (2003) 9–18.
[31] P. Gonon, E. Gheeraert, A. Deneuville, L. Abello, G. Lucazeau, Characterization of heavily B-doped polycrystalline diamond films using Raman spectroscopy and electron spin resonance, J. Appl. Phys. 78 (1995) 7059–7062.
[32] J.W. Ager, W. Walukiewicz, M. McCluskey, M.A. Plano, M.I. Landstrass, Fano interference of the Raman phonon in heavily boron-doped diamond films grown by chemical vapor deposition, Appl. Phys. Lett. 6 (1995) 616–618.
[33] R. Locher, J. Wagner, F. Fuchs, M. Maier, P. Gonon, P. Koidl, Optical and electrical characterization of boron-doped diamond films, Diam. Relat. Mater. 4 (1995) 678.
[34] K. Ushizawa, K. Watanabe, T. Ando, I. Sakaguchi, M. Nishitani-Gamo, Y. Sato, H. Kando, Boron concentration dependence of Raman spectra on {100} and {111} facets of B-doped CVD diamond, Diam. Relat. Mater. 7 (1998) 1719–1722.
[35] G. Faggio, G. Messina, S. Santangelo, G. Prestopino, I. Ciancaglioni, M. Marinelli, Raman scattering in boron-doped single-crystal diamond used to fabricate Schottky diode detectors, J. Quant. Spectrosc. Radiat. Transf. 113 (2012) 2476–2481.
[36] U. Fano, Effects of configuration interaction on intensities and phase shifts, Phys. Rev. 124 (1961) 1878—1886.
[37] E. Gheeraert, A. Deneuville, J. Mambou, Influence of diborane on the growth rate and phase stability of diamond films, Carbon 73 (1999) 107–111.
[38] R.J. Zhang, S.T. Lee, Y.W. Lam, Characterization of heavily boron-doped diamond films, Diam. Relat. Mater. 5 (1996) 1288–1294.
[39] B. Massarani, J.C. Bourgoin, R.M. Chrenko, Hopping conduction in semiconducting diamond, Phys. Rev. B 17 (1978) 1758–1769.
[40] F. Cleri, P. Keblinski, L. Colombo, D. Wolf, S.R. Phillpot, On the electrical activity of sp^2-bonded grain boundaries in nanocrystalline diamond, Europhys. Lett. 46 (1999) 671–677.
[41] B. Fiegl, R. Kuhnert, M. Ben-Chorin, F. Koch, Evidence for grain boundary hopping transport in polycrystalline diamond films, Appl. Phys. Lett. 65 (1994) 371–373.
[42] P. Keblinski, D. Wolf, F. Cleris, R. Phillpot, H. Gleitei, On the nature of grain boundaries in nanocrystalline diamond, MRS Bull. 23 (1998) 36–41.
[43] C.S. Fuller, J.A. Ditzenberger, Diffusion of lithium into germanium and silicon, Phys. Rev. 91 (1953) 193.